Versão do arquivo anexado / Version of attached file:

Versão do Editor / Published Version

Mais informações no site da editora / Further information on publisher's website:

https://journals.aps.org/prd/abstract/10.1103/PhysRevD.95.124040

DOI: 10.1103/PhysRevD.95.124040

Direitos autorais / Publisher's copyright statement:

Stability aspects of relativistic thin magnetized disks

Vanessa P. de Freitas[*]

Centro Brasileiro de Pesquisas Físicas, 22290-180 Rio de Janeiro, Rio de Janeiro, Brazil

Alberto Saa[†]

Departmento de Matemática Aplicada, IMECC–UNICAMP, 13083-859 Campinas, Sao Paulo, Brazil

We adapt the well-known "displace, cut and reflect" method to construct exact solutions of the Einstein-Maxwell equations corresponding to infinitesimally thin disks of matter endowed with dipole magnetic fields, which are entirely supported by surface polar currents on the disk. Our starting point is the Gutsunaev-Manko axisymmetric solution describing massive magnetic dipoles in general relativity, from which we obtain a continuous three-parameter family of asymptotically flat static magnetized disks with finite mass and energy. For strong magnetic fields, the disk surface density profile resembles some well-known self-gravitating ringlike structures. We show that many of these solutions can be indeed stable and, hence, they could be in principle useful for the study of the abundant astrophysical situations involving disks of matter and magnetic fields.

I. INTRODUCTION

Axially symmetric solutions of the Einstein equations corresponding to thin disks of matter are rather common in the physical literature. They can be static or stationary, with or without radial pressure, accommodate heat flow, electric charge, and halos, among many other possibilities, see, for instance [1–16]. Many of the known thin disk solutions can be obtained by using the so-called "displace, cut and reflect" (DCR) method, initially due to Kuzmin [17], which, in fact, has Newtonian origin and will be briefly presented in the next section. Matter disks and other self-gravitating structures in the presence of magnetic fields are particularly relevant due to the abundance of possible astrophysical applications, and there are indeed some previous examples of these solutions in the literature [18–21].

In the present work, we will show how to adapt the standard DCR method to generate consistent solutions of the Einstein-Maxwell equations corresponding to thin disks of matter with magnetic fields entirely supported by polar surface currents on the disk, a situation clearly mimicking realistic astrophysical thin plasma disks [22]. Our starting point will be the Gutsunaev-Manko two-parameter family of solutions describing massive axisymetric objects endowed with a magnetic dipole moment in general relativity [23–25]. In contrast with other solutions with magnetic fields, as for instance the long-standing and well-known one due to Bonnor [26], for the Gutsunaev-Manko family, the object mass and dipole magnetic moment are really independent quantities and, hence, we are able to generate a continuous three-parameter family of magnetized disks with finite total

mass and energy. The three parameters can determine univocally, for instance, the disk total mass, dipole magnetic moment, and central superficial density. Such parameters can be chosen to achieve some desired physical properties, with special emphasis, of course, to the stability of the solution. For the stability analysis of the disk, we consider, besides the usual generalized radial Rayleigh criteria [27,28], also the vertical stability (oblique orbits) [29]. We show that one indeed has a large continuous family of magnetized disks satisfying these stability criteria, which could be useful, in principle, for the study of the abundant astrophysical situations involving disks of matter and magnetic fields. Our magnetized disks have only azimuthal pressure, and hence they can be interpreted physically as composed by counterrotating particles, see, for instance, [10] for further references on this rather common hypothesis for static disks configurations in general relativity. Incidentally, we notice that there are indeed some recent observational evidences for counterrotating stellar disk, see [30,31] and references therein.

This article is organized as follows. Section II provides an overview of the DCR method and its necessary adaptation to generate viable magnetized disks. For sake of completeness, we also review briefly the main pertinent results about the stability of thin disks. Section III is devoted to construct and discuss the stability of the new solutions, and the last section is left for some concluding remarks about the stability of our disks.

II. RELATIVISTIC THIN DISKS

The Kuzmin "displace, cut and reflect" (DCR) method [17] can be used to generate rather generic thin disk configurations starting from a given solution of Einstein

---
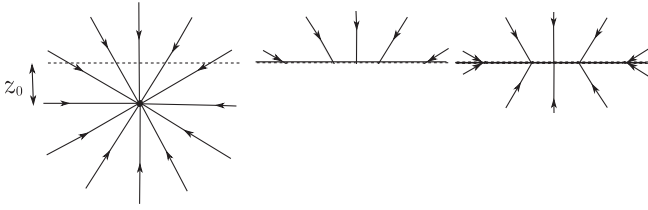[*]vpachecof@gmail.com
[†]asaa@ime.unicamp.br

FIG. 1. Illustration of the "displace, cut and reflect" (DCR) Kuzmin method starting from a central field in cylindrical coordinates. First, one chooses a hypersurface (dashed line) separating the spacetime in two regions (left), then we discard the part containing the source singularity (middle), and finally reflect the field on the hypersurface (right).

(or even Laplace) equations. Considering, for instance, a point-source solution, we can divide this method accordingly to the following steps: first we choose a hypersurface ($z = z_0$ in cylindrical coordinates, in our case, see Fig. 1) separating the spacetime in two regions, one of them containing the source of the gravitational field. Second, we discard the part that contains the source and, third, use the hypersurface $z = z_0$ to reflect the remaining part. The result of the application of this procedure will be generically a regular spacetime with a surface singularity or, in other words, a solution of Einstein equations with an infinite thin disk of matter located at $z = z_0$. Despite of being infinite, in many cases, as in the present one, these disks have finite total mass and energy and, hence, they might be considered as approximations to some finite size disks. The DCR procedure is fully equivalent to make the following mathematical transformation [15]:

$$z \to |z| + z_0 \qquad (1)$$

for all the pertinent quantities, where the disk plane now will be given by $z = 0$ and $z_0 > 0$ is a free parameter. Such a method can be applied virtually to any gravitational solution, relativistic or Newtonian, resulting generically in gravitational fields supported by surface distributions of matter, see [32] for further references.

We are mainly interested here in axisymmetric static solutions of the Einstein equations, and these solutions can be conveniently described in cylindrical coordinates (t, r, z, φ) as

$$
\begin{aligned}
ds^2 &= g_{\mu\nu}dx^\mu dx^\nu \\
&= e^{\psi(r,z)}dt^2 - e^{\eta(r,z)}(dr^2 + dz^2) - r^2 e^{\gamma(r,z)}d\varphi^2.
\end{aligned} \qquad (2)
$$

The application of (1) gives origin generically to functions of class C^0 across the disk plane. Using the standard notation $[f] = f|_{z=0^+} - f|_{z=0^-}$ for the discontinuities across the hypersurface $z = 0$, one has $[g_{\mu\nu}] = 0$. On the other hand, the z derivative of the metric tensor is typically discontinuous at $z = 0$, and the quantities

$$[\partial_z g_{\mu\nu}] = b_{\mu\nu} \qquad (3)$$

will determine all the physical and geometrical properties of the disk. In particular, the Christofel symbols and the Riemann curvature tensor $R^\sigma{}_{\alpha\gamma\beta}$ can be define by means of distributions involving (3), leading to [33]

$$R^\sigma{}_{\alpha\gamma\beta} = \mathcal{R}^\sigma{}_{\alpha\gamma\beta} + H^\sigma{}_{\alpha\gamma\beta}\hat{\delta}(z), \qquad (4)$$

where $\hat{\delta}(z)$ stands for the covariant Dirac δ-function [29], $R^\sigma{}_{\alpha\gamma\beta}$ is the (smooth) Riemann curvature tensor for $z \neq 0$, and

$$H^\sigma{}_{\alpha\gamma\beta} = \frac{e^{\eta/2}}{2}(\delta^z_\alpha \delta^z_\gamma b^\sigma_\beta - g^{z\sigma}\delta^z_\gamma b_{\alpha\beta} - \delta^z_\alpha \delta^z_\beta b^\sigma_\gamma + g^{z\sigma}\delta^z_\beta b_{\alpha\gamma}). \qquad (5)$$

From the contractions of (5), one can calculate directly the disk energy momentum tensor $Q_{\alpha\beta}$, which will be given by

$$H_{\alpha\beta} - \frac{1}{2}g_{\alpha\beta}H = 8\pi Q_{\alpha\beta}, \qquad (6)$$

with $H_{\alpha\beta} = H^\sigma{}_{\alpha\sigma\beta}$ and $H = H^\gamma{}_\gamma$. One finally has [29]

$$
\begin{aligned}
Q^\alpha_\beta = \frac{e^{\eta/2}}{16\pi}[&b^{z\alpha}\delta^z_\beta b^{zz}\delta^\alpha_\beta + g^{z\alpha}b^z_\beta - g^{zz}b^\alpha_\beta \\
&+ b^\sigma_\sigma(g^{zz}\delta^\alpha_\beta - g^{z\alpha}\delta^z_\beta)],
\end{aligned} \qquad (7)
$$

which is diagonal for metrics of the type (2). Its components correspond to the surface energy density and the pressures in the radial, axial, and azimuthal directions, respectively,

$$Q^\alpha_\beta = \mathrm{diag}(\sigma, -P_r, -P_z, -P_\varphi). \qquad (8)$$

Moreover, is clear from (7) that $P_z = 0$ for our case, as one would indeed naturally expect for infinitesimally thin disks. Assuming the system to be symmetric under reflections $z \to -z$, one can calculate σ, P_r, and P_φ for static axisymmetric spacetimes with metric (2), leading to [29]

$$\sigma = -\frac{e^{-\eta/2}}{8\pi}\left(\frac{\partial\gamma}{\partial|z|} + \frac{\partial\eta}{\partial|z|}\right)_{z=0}, \qquad (9)$$

$$P_r = \frac{e^{-\eta/2}}{8\pi}\left(\frac{\partial\psi}{\partial|z|} + \frac{\partial\gamma}{\partial|z|}\right)_{z=0}, \qquad (10)$$

$$P_\varphi = \frac{e^{-\eta/2}}{8\pi}\left(\frac{\partial\psi}{\partial|z|} + \frac{\partial\eta}{\partial|z|}\right)_{z=0}, \qquad (11)$$

where the notation $\frac{\partial}{\partial|z|}$ means that the derivative is calculated after the substitution (1). We are now in conditions to formulate the stability criteria we will use for the disk.

However, before starting the stability discussion, it is important to stress that the use of (1) alone is not enough to generate viable magnetized disks. The problem is that in the same way the DCR method induces a superficial density of matter at $z = 0$, it will generically do with a superficial density of magnetic monopoles on the disk [34], jeopardizing any possible realistic physical application for these solutions. Fortunately, this can be easily fixed. Suppose we have a solution of the Einstein-Maxwell equations of the form (2) with a magnetic field given by the electromagnetic quadripotential

$$A_\mu = [0, 0, 0, A_\varphi(r, z)]. \tag{12}$$

The linearity of the Maxwell equations and the quadratic structure of the Maxwell energy-momentum tensor imply that both A_μ and $-A_\mu$ are solutions of the Einstein-Maxwell equations for the same metric tensor (2). One can avoid the appearance of magnetic monopoles on the disk if we combine (1) with the transformation

$$A_\mu \rightarrow (\text{sgn } z) A_\mu. \tag{13}$$

By using (1) and (13), we will be able to generate disks of matter with dipole magnetic fields entirely supported by surface polar currents on the disk. Since the metric tensor is invariant under (13), the stability analysis, based solely in the energy-momentum tensor of the disk, is not affected by this transformation. On the other hand, (13) is crucial to obtain the polar currents which indeed generate the disk magnetization.

A. Disk stability conditions

As we will see, the matter content of our disks has no radial pressure, and in this case the disk is usually viewed as being composed of counterrotating identical particles, which guarantees, besides the vanishing of the radial pressure, a vanishing total angular momentum for the disk, despite the rotation of its matter content, see [10] for further details and references. We will perform two stability tests for our solutions: radial and vertical perturbations. In fact, they consist in the (linear) stability analysis of the circular orbits at $z = 0$ against small perturbations, and both tests can be derived from the geodesic motion on the disk plane and around its vicinity. Since (2) is static and axisymmetric, its geodesic equations will have two independent constants of motion: the total energy H and the angular momentum around the z direction L_z. The (reduced) Hamiltonian for the geodesics of the metric (2) is given by [29]

$$H^2(r, z, p_r, p_z) = e^{\psi - \eta}(p_r^2 + p_z^2) + V_{\text{eff}}(r, z), \tag{14}$$

where the effective potential

$$V_{\text{eff}}(r, z) = e^\psi \left(1 + e^{-\gamma} \frac{L_z^2}{r^2}\right) \tag{15}$$

will be crucial for both stability tests.

A pertinent and rather deep question is if this kind of stability analysis of the circular geodesics in the disk plane would be enough to guarantee the disk stability beyond the counterrotating hypothesis. A full answer to this question is obviously out of scope of the present paper, but we will return to this point in the last section.

1. The Rayleigh criterion

The Rayleigh criterion establishes the requirements for the circular orbits on the disk be stable against radial perturbations. Its relativistic version has been intensively studied in recent years, see [29]. Essentially, it can be deduced from the behavior of circular planar solutions of (14), *i.e.*, the solutions with $z = p_z = p_r = 0$ and, consequently, $r = \bar{r}$ constant, which, of course, occurs for $\partial_r V_{\text{eff}}(\bar{r}, 0) = 0$. The stability of such circular orbits requires

$$\frac{\partial^2 V_{\text{eff}}}{\partial r^2} = \frac{\partial_r e^\psi}{L_z^2} \partial_r L_z^2 > 0 \tag{16}$$

for all r, where

$$L_z^2 = \frac{r^4 e^{2\gamma} \partial_r e^\psi}{e^\psi \partial_r (r^2 e^\gamma) - r^2 e^\gamma \partial_r e^\psi} \tag{17}$$

is evaluated at $z = 0$. As one can see, the disk radial stability requires that both e^ψ and L_z^2 be monotonically increasing functions of r on the disk plane $z = 0$. The situation here is clearly analogous to the Newtonian case [17,35].

2. Vertical stability

Since the dynamics of the geodesics are in fact singular at $z = 0$, the stability of the oblique orbits will be determined solely by the "restoring" vertical force $\partial_{|z|} V_{\text{eff}}$ [29]. In fact, for the metric (2), the condition

$$\frac{\partial V_{\text{eff}}}{\partial |z|} = 4\pi e^{\psi + \eta/2} \left[P_r + \left(1 + \frac{2L_z^2}{r^2 e^\gamma}\right)(\sigma + P_\varphi) \right] > 0, \tag{18}$$

evaluated on the plane $z = 0$, is enough to guarantee the vertical stability of circular orbits in our disks.

III. MAGNETIZED DISKS

The Gutsunaev-Manko spacetimes [23–25] form a large family of asymptotically flat, axisymmetric, and stationary solutions of the Einstein-Maxwell equations. We are mainly interested here in one of their simplest subcases, the continuous two-parameter family corresponding to the

gravitational field of massive magnetic dipoles [24]. It can be conveniently written, using the cylindrical coordinates (2), in the Weyl line element form, for which

$$e^\psi = e^{-\gamma} = \frac{x-1}{x+1} f^2, \tag{19}$$

and

$$e^\eta = \frac{(x+1)^2}{x^2 - y^2} \left(\frac{g}{f}\right)^2, \tag{20}$$

with

$$f = \frac{(x^2 - y^2 + \alpha^2(x^2 - 1))^2 + 4\alpha^2 x^2(1 - y^2)}{(x^2 - y^2 + \alpha^2(x-1)^2)^2 - 4\alpha^2 y^2(x^2 - 1)} \tag{21}$$

and

$$g = \left(\frac{(x^2 - y^2 + \alpha^2(x^2 - 1))^2 + 4\alpha^2 x^2(1 - y^2)}{(1 + \alpha^2)^2 (x^2 - y^2)^2}\right)^2, \tag{22}$$

where α is a dimensionless constant, and x and y are the usual prolate coordinates, related to the cylindrical coordinates r and z by

$$x = \frac{1}{2k}\left(\sqrt{r^2 + (z+k)^2} + \sqrt{r^2 + (z-k)^2}\right), \tag{23}$$

$$y = \frac{1}{2k}\left(\sqrt{r^2 + (z+k)^2} - \sqrt{r^2 + (z-k)^2}\right), \tag{24}$$

where k is a dimensional constant. The dipole magnetic field, which has the form (12), is given by

$$A_\varphi = \frac{4k\alpha^3}{1+\alpha^2}(1-y^2)$$
$$\times \frac{2(1+\alpha^2)x^3 + (1-3\alpha^2)x^2 + y^2 + \alpha^2}{(x^2 - y^2 + \alpha^2(x^2-1))^2 + 4\alpha^2 x^2(1-y^2)}. \tag{25}$$

In order to interpret the physical role of the two parameters k and α, one can cast the metric in spherical coordinates and analyze the asymptotically flat limit [23–25], leading to the conclusion that these parameters are related to the mass m and magnetic dipole μ of the central object by the expressions

$$m = \frac{1 - 3\alpha^2}{1 + \alpha^2} k, \tag{26}$$

$$\mu = \frac{8\alpha^3}{(1+\alpha^2)^2} k^2. \tag{27}$$

The only restrictions on these parameters in order to have physically meaningful solutions, for our purposes, are

$k > 0$ and $3\alpha^2 < 1$. The Schwarzschild case is recovered for $\alpha = 0$, and the solution can accommodate any values for the mass m and the dipole magnetic moment μ. In particular, α is given by

$$\frac{8\alpha^3}{(1-3\alpha^2)^2} = \frac{\mu}{m^2}, \tag{28}$$

from where it is clear that with $3\alpha^2 < 1$ one can effectively cover all possibilities for μ and m. The parameter α is clearly dimensionless, k is the only massive parameter for these solutions. All the dimensional quantities in our analysis will be always expressed in units of k. The Gutsunaev-Manko solutions are asymptotically flat, and such a crucial property will be inherited by our disks.

The magnetized disks are generated by doing the transformation (1) and simultaneously $\alpha \to -\alpha$, which implements (13), in all pertinent expressions, giving origin to a three-parameter (k, α, z_0) family of disk solutions for the Einstein-Maxwell equations. We will restrict ourselves to configurations such that $z_0 > k$ in order to avoid the rather intricate causal structure of the Gutsunaev-Manko solution near its center; otherwise, it would be impossible to have stable disk configurations. We will return to this point in the last section. Despite all pertinent expressions here involve essentially only rational functions and, hence, all the calculations can be straightforwardly carried out, the resulting expressions are quite cumbersome, and so we opt to present our results graphically. Nevertheless, we present in the Appendix all the necessary details to evaluate the algebraic expressions. The explicit expressions for the Gutsunaev-Manko solutions allow some useful simplifications. In particular, since $\psi = -\gamma$, see (19), one gets from (10) that, as we have already advanced, $P_r = 0$, reducing the vertical stability criterion to

$$\sigma + P_\varphi = \frac{e^{-\psi - \eta/2}}{4\pi} \frac{\partial e^\psi}{\partial |z|} > 0, \tag{29}$$

at $z = 0$, or, in other words, the disk must obey the null energy condition to assure the stability of vertical perturbations (oblique orbits). Hence, we will guarantee both the radial and vertical stabilities provided that, on the disk plane $z = 0$, $\partial_{|z|} e^\psi$ is a positive function, and e^ψ and

$$L_z^2 = \frac{r^3 \partial_r e^\psi}{2e^{2\psi} - r\partial_r e^{2\psi}} \tag{30}$$

are monotonically increasing in r, see (16).

Let us start with the function e^ψ given by (19). It is indeed monotonically increasing in r on the disk plane $z = 0$ for large ranges of the parameters. The asymptotic behavior of e^ψ, see (14) in the Appendix, assures its monotonic character for large r, for any value of the parameters. Figure 2 depicts some typical cases around the disk central region. As one can
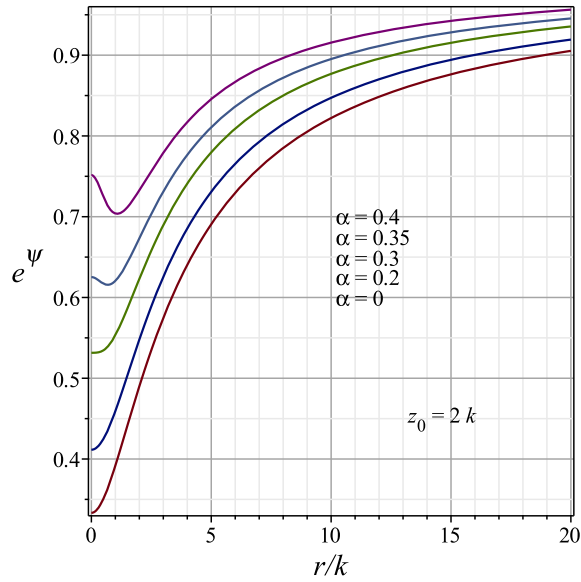
FIG. 2. Typical aspect of the function e^ψ given by (19) on the disk plane $z = 0$, here depicted for $z_0 = 2k$ and several values of α, with the respective curves from bottom to top. The non-monotonic behavior is associated with the concavity change of the function e^ψ at the origin, see the text.
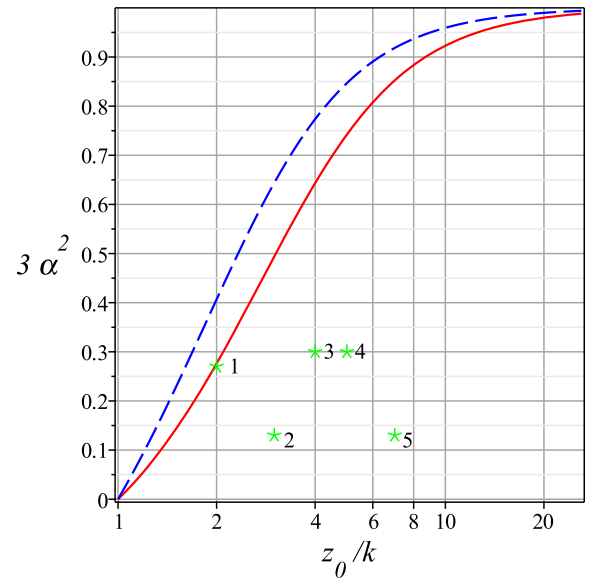

FIG. 3. Diagram $3\alpha^2$ versus z_0/k (monolog scale). The red (solid) line corresponds to the threshold α_* for monotonically increasing functions e^ψ, see Fig. 2. Only points lying below this curve are allowed for stable circular obits on the disk. The blue (traced) line corresponds to the values of α and z_0 such that the disk central density σ_0 vanishes. In order to have a positive σ_0, the parameters α and z_0 must lay below this curve. As one can see, is enough to have a monotonically increasing e^ψ to assure a positive σ_0. The green numbered points correspond to some typical disk configurations presented in the next figures and discussed in the text. Their $(z_0/k, \alpha)$ values are, respectively: (2, 0.30), (3, 0.21), (4, 0.32), (5, 0.32), and (7, 0.21).

see, the function fails to be monotonically increasing for some larger values of α. For a given z_0, one needs to restrict α to a certain interval $(-\alpha_*, \alpha_*)$ in order to have a monotonic e^ψ. We can check that $\partial_r e^\psi = 0$ at $r = z = 0$ for all values of the parameters α and z_0. The nonmonotonic phase is associated with the concavity change of the function e^ψ at the origin. In order to determine the value of α_* as a function of z_0 associated with this concavity change, one needs to find the roots of a cumbersome higher order polynomial, so again we employ numerical and graphical analyses. (See the Appendix for the details on the algebraic expressions.) Figure 3 shows the interval limit α_* as a function of z_0. Viable disks must have the parameters (z_0, α) lying below the depicted red (solid) curve.

The parameter z_0 can be related to the disk surface density, which in our case is given by

$$\sigma = \frac{e^{-3\eta/2 - \psi}}{8\pi} \left(e^\eta \frac{\partial e^\psi}{\partial |z|} - e^\psi \frac{\partial e^\eta}{\partial |z|} \right). \quad (31)$$

Let us consider the central ($r = 0$) disk density σ_0, which one can evaluate directly as

$$\sigma_0 = \frac{1}{2\pi k} \sqrt{\frac{z_0 - k}{z_0 + k}} \left(f_x^{(0)} + \frac{k^2 f^{(0)}}{z_0^2 - k^2} \right), \quad (32)$$

where the $^{(0)}$ superscript indicates that the corresponding quantities are calculated at the center of the disk. This calculation is rather tedious, but straightforward, the details are in the Appendix. For fixed α and large z_0, one has

$$\sigma_0 \sim \frac{mk}{2\pi z_0^2}, \quad (33)$$

where m is the mass given by (26). Hence, the central surface density σ_0 decreases when z_0 increases for fixed α, i.e., the disk becomes fainter, as one would indeed expect from the DCR method applied for an asymptotically flat spacetime. The problem, however, is that for a fixed z_0, there are values of α such that $\sigma_0 < 0$, challenging the idea that the disk would be formed by some kind of ordinary counter-rotating matter. One can determine the values of α such that, for a given z_0, the term between parenthesis in (32) change its signal. The results are also depicted in Fig. 3. It is important to stress that the values of α which leads to a negative σ_0 are always larger than those ones assuring a monotonic function e^ψ, see Fig. 2. Hence, a monotonically increasing e^ψ will also guarantee a positive central disk superficial density σ_0. Furthermore, from (31), we have for large r

$$\sigma \sim \frac{m z_0}{2\pi r^3}, \quad (34)$$

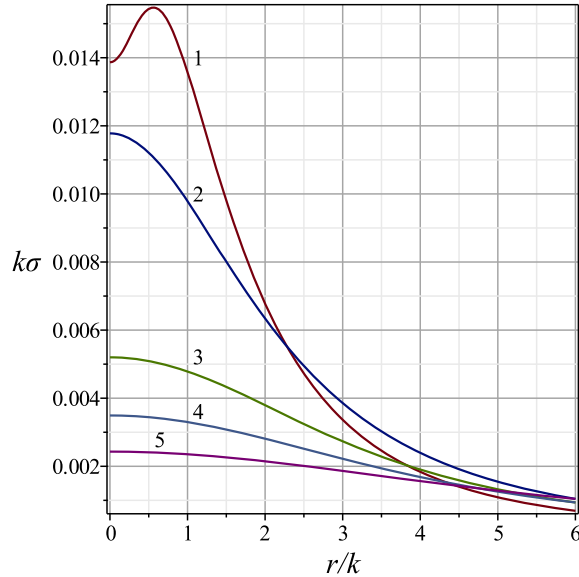and, consequently, the total mass of the disk will be always finite.

FIG. 4.   Disk surface density σ given by (31) as a function of r, for the disk configurations described in Fig. 3. For strong magnetic fields (larger α, as for the case of the configuration number 1), the maximum of the surface density is located at a $r > 0$, suggesting a ringlike distribution.

FIG. 5.   The squared angular momentum in the z direction L_z^2, given by (30), for a circular orbit on the disk, as a function of r. The curves correspond to the disk configurations enumerated in Fig. 3. It is clear that we have a monotonically increasing function of r for all curves.

It is instructive also to inspect the graphics of the disk surface energy density (31), see Fig. 4. For configurations near the concavity threshold [red (solid) line in Fig. 3], as for instance the configuration number 1, the maximum density of the disk is not located at its center, but at a certain radius $r_* > 0$, typically smaller than z_0. This kind of configuration resembles clearly some well known self-gravitating ring structures, see [36] for references. In our case, such rings require strong magnetic fields to exist. For weak magnetic fields (small α), the maximum of the surface density will be always located at the disk center.

The Rayleigh criterion for radial stability demands that both e^ψ and L_z^2 be monotonically increasing functions of r on the disk plane. Figure 5 depicts the aspect of the function L_z^2 in the disk central region. Since we have $L_z^2 \sim mr$ for large r, we conclude from Fig. 5 that the allowed configurations (see Fig. 3) are indeed radially stable. It is interesting also to inspect the aspect of the effective radial potential (15) on the disk center, see Fig. 6. For large r, we have $V_{\rm eff} \sim 1 - m/r$. It is clear that we can have radially stable noncircular motion as well.

Finally, one needs to check the vertical stability criterion, namely the positivity of $\partial_{|z|} e^\psi$ on the disk plane. However, it turns out that the aspect of the function $\partial_{|z|} e^\psi$ is very similar to the surface density (4) depicted in Fig. 4, including the appearance of some maxima at $r_* > 0$ for large values of α. Nevertheless, for the allowed configurations [those ones lying below the red (solid) line in Fig. 3], this function is always positive, assuring both the radial and vertical stability of circular orbits in our disks.
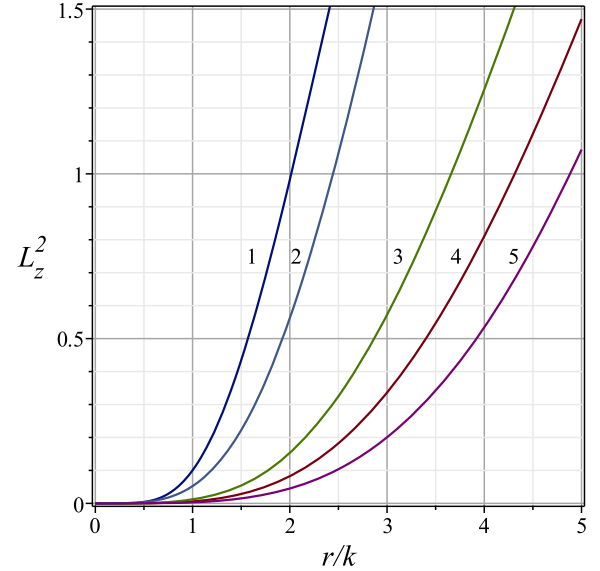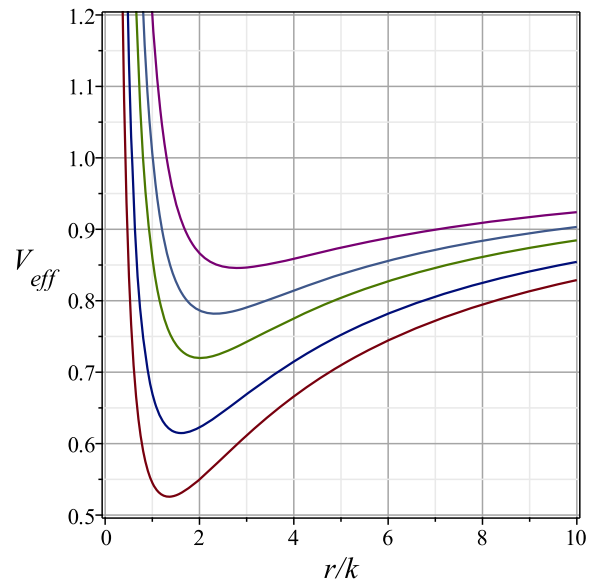

FIG. 6.   The effective potential $V_{\rm eff}$ given by Eq. (15) for the disk configurations of Fig. 2, with the curves disposed from top to bottom, and $L_z^2 = 1$. Other values for L_z^2 will only change the repulsive behavior near the origin. The circular orbits at $\bar{r}$ correspond to the minimum of $V_{\rm eff}$. It is clear that we can have radially bounded motion around $\bar{r}$.

A. The disk surface currents

Since our disks have dipole magnetic fields, it is mandatory to investigate their origin. We will see that the magnetic fields are supported entirely by surface polar

currents on the disk plane. Notice that for the electromagnetic quadripotential (12), the nonvanishing components of the electromagnetic tensor are $F_{\varphi r} = -F_{r\varphi} = \partial_r A_\varphi$ and $F_{\varphi z} = -F_{z\varphi} = -\partial_z A_\varphi$. The former is associated with the magnetic field B_z in the z direction, while the latter is its radial component B_r. The application of (1) without (13) would produce a discontinuous B_z across the disk plane $z = 0$, while B_r would be continuous. Such kind of discontinuity would lead unavoidably to a nonvanishing divergence for the magnetic field, implying the annoying presence of magnetic monopoles on the disk plane, see [34] for further details on this issue. By applying simultaneously (1) and (13), the magnetic monopoles are avoided, since now the normal component of the magnetic field B_z is continuous across the disk plane, while the discontinuity is restricted to the radial part B_r. However, such a discontinuity in the parallel direction of the disk plane is not a problem at all, since it can be explained naturally due to the presence of superficial currents on the disk. In fact, the nonhomogeneous Maxwell equation

$$\frac{1}{\sqrt{-g}} \partial_\mu \sqrt{-g} F^{\mu\nu} = 4\pi J^\nu \qquad (35)$$

can be invoked here to determine the surface current j_φ such that

$$J^\nu = g^{\nu\varphi} j_\varphi \hat{\delta}(z), \qquad (36)$$

where $\hat{\delta}(z)$ stands for the covariant Dirac δ-function. Applying the divergence theorem in (35) and taking into account that the parallel component of the magnetic field is discontinuous, one has

$$j_\varphi = \frac{e^{-\eta/2}}{2\pi} \frac{\partial A_\varphi}{\partial |z|}, \qquad (37)$$

leading to the invariant

$$j^2 = j_\varphi j^\varphi = \frac{e^{\psi-\eta}}{4\pi^2 r^2} \left(\frac{\partial A_\varphi}{\partial |z|}\right)^2, \qquad (38)$$

which aspect is illustrated in Fig. 7 for the disk configurations considered in Fig. 3. Notice that, for large r, we have (see the Appendix for details on the asymptotic analysis) the following asymptotic behavior for the current invariant:

$$j^2 \sim \frac{9\mu^2 z_0^2}{4\pi^2 r^8}, \qquad (39)$$

implying that the total electromagnetic energy stored in the disk surface currents is finite. Also from Fig. 7, one can see that the surface current is always distributed in a smooth ringlike structure, irrespective of the disk superficial
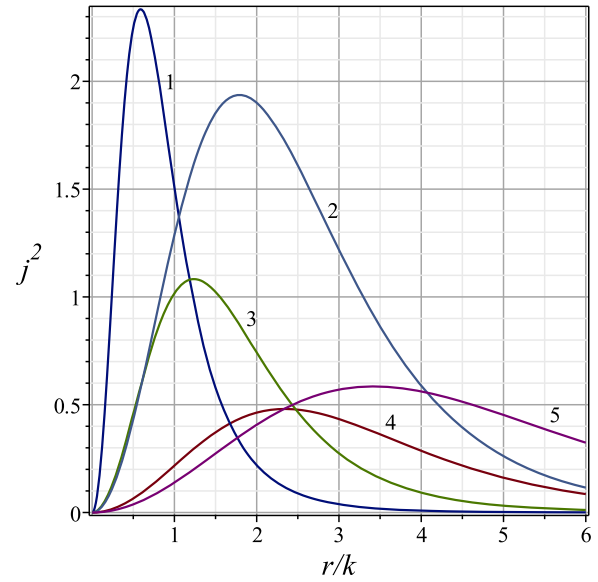

FIG. 7. The surface electric current invariant $j^2 (\times 10^7)$ given by (38), as a function of r for the allowed disk configurations of Fig. 3. The curves corresponding to the configurations number 1 and 5 are rescaled to fit in the graphics. They are, respectively, multiplied by 10^{-2} and 10^2.

density. The maximum of j^2 is typically located at a radius $r > 0$ smaller than z_0, suggesting strongly that the ringlike structure in the energy density profile of Fig. 4 has its origin precisely in the surface currents.

IV. FINAL REMARKS

Starting from the Gutsunaev-Manko solution [23–25] describing massive magnetic dipoles in general relativity, we have generated a continuous three-parameter family of solutions corresponding to static magnetized thin disks. We have adapted the well known "displace, cut and reflect" DCR method, due to Kuzmin [17], to avoid the presence of magnetic monopoles on the disk. Essentially, we combine with the usual steps of the DCR method the reflection (13) on the electromagnetic potential. In this way, we obtain a field configuration such that the magnetic field component B_z perpendicular to the disk is continuous, whereas the parallel component B_r is discontinuous, leading to a physical situation without magnetic monopoles, but with the magnetic field entirely supported by surface polar currents. Moreover, all disk solutions such that the parameters (z_0, α) are in the allowed region (laying below the red (solid) curve in Fig. 3) have circular obits stable against radial and vertical perturbations. Since our disks have no radial pressure, it can be considered as formed by counterrotating identical particles, and them the stability of circular orbits is essential to establish the stability of the solution.

A certainly pertinent question here is if the two stability test we have performed would be enough to assure the stability of the disk beyond the counterrotating hypothesis.

This is quite complicated problem. Since the matter content of the disk has azimuthal pressure, the motion of its constituents will not be purely geodesic as one would expect, for instance, for real dust disks (no pressure at all). The stability analysis of the disk fluid does require extra information like, for instance, the fluid equation of state, see [37]. Also, the dynamics of oblique orbits in disks with central fields is known to be generically chaotic [38–45], challenging the view that the counterrotating particles will keep their circular orbits for long times. These are more subtle question that we can now put forward once we have established that our magnetized disks pass by the simplest stability tests. Our results are, in this sense, the first step to a deeper study of the stability of these disks.

Finally, we have restricted the application of the DCR method for the cases where $z_0 > k$. In order to enlighten such an option, let us consider the inverse of the transformations (23) and (24), namely

$$r = k\sqrt{x^2 - 1}\sqrt{1 - y^2}, \tag{40}$$

$$z = kxy. \tag{41}$$

Recalling that the prolate coordinates are such that $x \geq 1$ and $-1 \leq y \leq 1$, we see that the vertical segment $|z| \leq k$ at the origin $r = 0$ corresponds to $x = 1$ and $|y| < 1$. However, for $x = 1$ we have $e^\psi = 0$, see (19), and so any disk constructed by choosing the hyperplane $z_0 < k$ will unavoidably encounter the complicated, and not yet quite well understood, causal structure of the central part of the Gutsunaev-Manko solution. In particular, it would be impossible to attain any stable configuration. The situation is analogous to the disks generated from Schwarzschild solution. Nevertheless, disk distributions approaching the horizon of generic black holes are certainly interesting for the study of accretion disks [36,46,47]. This is a rather promising possibility for our magnetized disks that would deserve further investigations since they might give some insights of possible observational signatures which one could seek, for instance, with the Event Horizon Telescope [48].

APPENDIX: MATHEMATICAL FORMULAS

The mathematical expressions in this work involve essentially only algebraic rational functions and, hence, the evaluation of derivatives and the location of zeros could, in principle, be straightforwardly done. Nevertheless, the resulting expressions are typically huge, and we have indeed taken advantage of MAPLE software to deal with them. However, we have some useful simplifications for the asymptotic analysis of large r and in the central region of the disk. The calculation of the disk central density (32), for instance, can be considerably simplified noticing that, at the disk center, which has prolate coordinates $x = \frac{z_0}{k}$ and $y = 1$, one has $g = 1$, $\frac{\partial x}{\partial |z|} = \frac{1}{k}$, and $\frac{\partial y}{\partial |z|} = 0$. The other relevant quantities at the disk center are

$$e^\psi = e^{-\eta} = \frac{z_0 - k}{z_0 + k} f^2, \tag{A1}$$

$$\frac{\partial e^\psi}{\partial |z|} = \frac{2kf^2}{(z_0 + k)^2} + \frac{2f}{k}\frac{z_0 - k}{z_0 + k}\frac{\partial f}{\partial x}, \tag{A2}$$

and

$$\frac{\partial e^\eta}{\partial |z|} = \frac{1}{f^2}\left(\frac{1}{k}\frac{z_0 + k}{z_0 - k}\left(\frac{\partial g^2}{\partial x} - \frac{2}{f}\frac{\partial f^2}{\partial x}\right) - \frac{2k}{(z_0 - k)^2}\right). \tag{A3}$$

It turns out that $\partial_x g^2$ vanishes at the disk center, as one can check after some algebra. Combining these results leads to

$$e^\eta\frac{\partial e^\psi}{\partial |z|} - e^\psi\frac{\partial e^\eta}{\partial |z|} = \frac{4k}{z_0^2 - k^2} + \frac{4}{kf}\frac{\partial f}{\partial x}, \tag{A4}$$

from where (32) follows directly. The values of f and f_x at the disk center, necessary to determine the zeros of (32), are

$$f^{(0)} = \frac{(1 + \alpha^2)^2(z_0^2 - k^2)^2}{(z_0^2 - k^2 + \alpha^2(z_0 - k)^2)^2 - 4\alpha^2 k^2(z_0^2 - k^2)}, \tag{A5}$$

and

$$f_x^{(0)} = 4\left(z_0 - \frac{1}{k^2}h^{(0)}f^{(0)}\right)f^{(0)}, \tag{A6}$$

where

$$h^{(0)} = (z_0 - k)^3\alpha^4 + (2z_0^3 - 3kz_0^2 - 2k^2 z_0 + k^3)\alpha^2$$
$$+ z_0^3 - k^2 z_0. \tag{A7}$$

The concavity analysis of e^ψ in Fig. 3 requires the evaluation of $\partial_r e^\psi$ and $\partial_r^2 e^\psi$ at the disk center, $r = z = 0$, or $x = \frac{z_0}{k}$ and $y = 1$. Since $\frac{\partial x}{\partial r} = \frac{\partial y}{\partial r} = 0$ at the disk center, we will also have $\partial_r e^\psi = 0$. For the second derivative, we have

$$\frac{\partial^2 x}{\partial r^2} = \frac{z_0/k}{z_0^2 - k^2} \tag{A8}$$

and

$$\frac{\partial^2 y}{\partial r^2} = -\frac{1}{z_0^2 - k^2} \tag{A9}$$

at $r = z = 0$, leading to

$$\partial_r^2 e^\psi = \frac{2f}{z_0^2 - k^2} \left(\frac{z_0^2}{k^2} \frac{f}{(z_0 + k)^2} + \frac{z_0 - k}{z_0 + k} \left(\frac{z_0}{k} \partial_x f - \partial_y f \right) \right),$$ (A10)

which can be calculated analogously to the case of $\frac{\partial e^\psi}{\partial |z|}$ above. The critical values α_*^2 of Fig. 3 are the roots of the higher order polynomial corresponding to $\partial_r^2 e^\psi = 0$ at $r = z = 0$.

For the asymptotic behavior of our solutions for large r on the disk plane $z = 0$, notice that from (23) and (24), we have that $x \sim \frac{r}{k}$ and $y \sim \frac{z_0}{r}$ for $z = 0$ and large r. For their derivatives, we have

$$\frac{\partial x}{\partial r} \sim \frac{1}{k}, \qquad \frac{\partial x}{\partial z} \sim \frac{z_0}{kr}, \qquad (A11)$$

$$\frac{\partial y}{\partial r} \sim \frac{z_0}{r^2}, \qquad \frac{\partial y}{\partial z} \sim \frac{1}{r}, \qquad (A12)$$

in the same asymptotic limit. From these asymptotic limits, one can get

$$e^\psi \sim 1 - \frac{2m}{r}, \qquad e^\eta \sim 1 + \frac{2m}{r} \qquad (A13)$$

$$\frac{\partial e^\psi}{\partial r} \sim -\frac{\partial e^\eta}{\partial r} \sim \frac{2m}{r^2} \qquad (A14)$$

$$\frac{\partial e^\psi}{\partial |z|} \sim -\frac{\partial e^\eta}{\partial |z|} \sim \frac{2mz_0}{r^3} \qquad (A15)$$

with m given by (26). For the magnetic potential (25), we have

$$\frac{\partial A_\varphi}{\partial |z|} \sim -\frac{24\alpha^3}{(1 + \alpha^2)^2} \frac{z_0 k^2}{r^3} = -\frac{3\mu z_0}{r^3}, \qquad (A16)$$

for large r at $z = 0$, with μ given by (27), from where (39) follows directly.

[1] W. B. Bonnor and A. Sackfield, Commun. Math. Phys. **8,** 338 (1968).

[2] T. Morgan and L. Morgan, Phys. Rev. **183,** 1097 (1969).

[3] L. Morgan and T. Morgan, Phys. Rev. D **2,** 2756 (1970).

[4] D. Lynden-Bell and S. Pineault, Mon. Not. R. Astron. Soc. **185,** 679 (1978).

[5] P. S. Letelier and S. R. Oliveira, J. Math. Phys. (N.Y.) **28,** 165 (1987).

[6] J. P. S. Lemos, Classical Quantum Gravity **6,** 1219 (1989).

[7] J. Bičák, D. Lynden-Bell, and J. Katz, Phys. Rev. D **47,** 4334 (1993).

[8] J. P. S. Lemos and P. S. Letelier, Classical Quantum Gravity **10,** L75 (1993).

[9] J. P. S. Lemos and P. S. Letelier, Phys. Rev. D **49,** 5135 (1994).

[10] G. A. González and O. A. Espitia, Phys. Rev. D **68,** 104028 (2003).

[11] G. García-Reyes and G. A. González, Phys. Rev. D **70,** 104005 (2004).

[12] J. Bičak and T. Ledvinka, Phys. Rev. Lett. **71,** 1669 (1993).

[13] G. A. González and P. S. Letelier, Phys. Rev. D **62,** 064025 (2000).

[14] G. A. González and P. S. Letelier, Classical Quantum Gravity **16,** 479 (1999).

[15] D. Vogt and P. S. Letelier, Phys. Rev. D **68,** 084010 (2003).

[16] D. Vogt and P. S. Letelier, Phys. Rev. D **70,** 064003 (2004).

[17] G. G. Kuzmin, Astron. Zh. **33,** 27 (1956).

[18] P. S. Letelier, Phys. Rev. D **60,** 104042 (1999).

[19] A. C. Gutiérrez-Piñeres, G. A. González, and H. Quevedo, Phys. Rev. D **87,** 044010 (2013).

[20] A. C. Gutiérrez-Piñeres, G. García-Reyes, and G. A. González, Int. J. Mod. Phys. D **23,** 1450010 (2014).

[21] B. H. Lee, W. Lee, and D. H. Yeom, Phys. Rev. D **92,** 024027 (2015).

[22] B. V. Somov, *Plasma Astrophysics, Part I*, Astrophysics and Space Science Library Vol. 391 (Springer, New York, 2013).

[23] T. I. Gutsunaev and V. S. Manko, Phys. Lett. **123A,** 215 (1987).

[24] T. I. Gutsunaev and V. S. Manko, Phys. Lett. **132A,** 85 (1988).

[25] T. I. Gutsunaev and V. S. Manko, Gen. Relativ. Gravit. **20,** 327 (1988).

[26] W. B. Bonnor, Z. Phys. **190,** 444 (1966).

[27] L. Rayleigh, Proc. R. Soc. A **93,** 148 (1917).

[28] P. S. Letelier, Phys. Rev. D **68,** 104002 (2003).

[29] R. S. S. Vieira, J. Ramos-Caro, and A. Saa, Phys. Rev. D **94,** 104016 (2016).

[30] F. Bertola, P. Cinzano, E. M. Corsini, A. Pizzella, M. Persic, and P. Salucci, Astrophys. J. Lett. **458,** L67 (1996).

[31] A. Subramaniam and T. P. Prabhu, Astrophys. J. Lett. **625,** L47 (2005).

[32] G. A. Gonzalez and P. S. Letelier, Phys. Rev. D **69,** 044013 (2004).

[33] A. H. Taub, J. Math. Phys. (N.Y.) **21,** 1423 (1980).

[34] N. Gurlebeck, J. Bicak, and A . C. Gutierrez-Pineres, Phys. Rev. D **83,** 124023 (2011).

[35] R. S. S. Vieira, J. Schee, W. Kluzniak, Z. Stuchlik, and M. Abramowicz, Phys. Rev. D **90,** 024035 (2014).

[36] L. Qian, M. A. Abramowicz, P. C. Fragile, J. Horak, M. Machida, and O. Straub, Astron. Astrophys. **498,** 471 (2009).

[37] M. Ujevic and P. S. Letelier, Phys. Rev. D **70**, 084015 (2004).

[38] A. Saa and R. Venegeroles, Phys. Lett. A **259**, 201 (1999).

[39] A. Saa, Phys. Lett. A **269**, 204 (2000).

[40] C. Hunter, *Galaxies and Chaos*, Lecture Notes on Physics Vol. 626, edited by G. Contopoulos and N. Voglis (Springer, New York, 2003), p. 137.

[41] C. Hunter, Ann. N.Y. Acad. Sci. **1045**, 120 (2005).

[42] O. Semerak and P. Sukova, Mon. Not. R. Astron. Soc. **404**, 545 (2010).

[43] O. Semerak and P. Sukova, Mon. Not. R. Astron. Soc. **425**, 2455 (2012).

[44] P. Sukova and O. Semerak, Mon. Not. R. Astron. Soc. **436**, 978 (2013).

[45] V. Witzany, O. Semerak, and P. Sukova, Mon. Not. R. Astron. Soc. **451**, 1770 (2015).

[46] O. Semerak, in *Gravitation: Following the Prague Inspiration (To Celebrate the 60th Birthday of Jiri Bicak)*, edited by O. Semerak, J. Podolsky, and M. Zofka (World Scientific, Singapore, 2002); arXiv:gr-qc/0204025.

[47] V. Karas, J. M. Hure, and O. Semerak, Classical Quantum Gravity **21**, R1 (2004).

[48] http://www.eventhorizontelescope.org/.